Plasma Chemistry and Plasma Processing, Vol. 20, No. 2, 2000

Use of Liquid Precursors for Diamond Chemical Vapor Deposition—The Effects of Mass Transport and Oxygen

Marcus Asmann,[1] Joachim Heberlein,[1] and Emil Pfender[1]

Received June 2, 1999; revised July 22, 1999

Thermal plasma chemical vapor deposition of diamond-utilizing liquid feedstock injection has been shown to yield higher mass deposition rates, larger crystal size, and thicker films when compared to the use of gaseous feedstock for equivalent operating conditions. Increased mass transport of the activated precursor species across the substrate diffusion boundary layer and the presence of oxygen in liquid precursors are investigated as potential reasons for the observed results. Comparisons of the various precursor systems investigated in this study are based on crystal size and film thickness as a function of radial postion, area of deposit, total mass deposition rate, and the observed liquid precursor droplet trajectories within the deposition chamber using a laser strobe video system. The results indicate that the mass transport in both the liquid and gaseous precursor systems is greatly improved by the use of an inert carrier gas. Further, the use of a liquid versus a gaseous precursor does not seem to result in higher total deposition rates when the operating conditions for both have been optimized. Finally, the presence of oxygen in the liquid feedstock system is found to be at least partly responsible for the increased growth rate, which is observed when comparing the plain hydrocarbon precursor cases with the oxygenated liquid precursor case.

KEY WORDS: Diamond CVD; liquid precursors; mass transport; oxygen.

1. INTRODUCTION

The use of liquid precursors, directly injected into a thermal plasma for activation in the diamond chemical vapor deposition system (CVD), has been shown to produce enhanced growth rates both in a side injection system,[(1–3)] and, in particular, in a counterflow injection system.[(2,4–7)] For the purpose of this article, activation is defined as covering those processes that produce species that directly or indirectly partake in the diamond CVD

[1]University of Minnesota, High Temperature and Plasma Technology Laboratory, Minneapolis, Minnesota 55455.

0272-4324/00/0600-0209$18.00/0

process. The particular enhancement of growth rates in the counterflow system are believed to be due to the injection geometry, as well as the properties of liquids. In the counterflow system, an atomizing gas is directly injected from the center of the substrate, counter to the plasma jet flow, into the plasma jet. The result of this counterflow scheme is full mixing of the precursor and torch gases,[8] leading to higher activation rates, as well as highly nonuniform substrate deposits.[2]

Even without the use of the counterflow system, enhanced growth rates have been observed with the use of liquid feedstock. Several reasons for the observed increase in growth rate in the liquid feedstock case exist. The presence of oxygen in most liquid precursors and the lack thereof in the common gaseous precursor, methane, used as a comparison, is one potential reason. Oxygen has been found to increase growth rates in numerous systems when added to the common carbon–hydrogen system.[9–12] Although the role of oxygen in increasing deposition rates has not been validated, an increase in atomic hydrogen concentration in the gas phase,[13,14] as well as the formation of OH and O radicals has been reported.[15–17] An increase in atomic hydrogen, as well as the presence of OH radicals, is believed to lead to an increase in active surface sites for diamond growth. In turn, increased active surface site concentrations lead to larger carbon deposition rates.

Another potential reason for the higher growth rates observed in the diamond CVD system utilizing liquid feedstock injection compared to gaseous feedstock can be related to an increase in mass transport across the substrate diffusion boundary layer enabled by the use of the liquid feedstock. Determination of the role of direct liquid feedstock injection and its effect on mass transport has been the focus of a liquid feedstock diamond CVD model developed by Kolman *et al.*[18–20] for the system under discussion in this article. Results indicate that liquid droplets actually evaporate and dissociate right above the fluid boundary layer of the substrate. As a consequence, high concentrations of active species are formed close to the substrate, which, in turn, induce increased product species mass transport across the diffusion boundary layer.

Other investigations of diamond CVD systems have concluded that film growth rates for systems with low nucleation densities are controlled by surface reaction rates,[21] while systems with high nucleation densities are believed to be limited by mass-transport rates.[21,22] Previous experiments have shown that the time for full film coverage is less than 5 min in the thermal plasma CVD system being investigated. Therefore film growth occurs under the condition of high nucleation density. The growth rate in the system under consideration is, therefore, believed to be mass transport limited. The introduction of packets of (oxygenated) hydrocarbon in the

form of droplets, should produce local increases in the hydrocarbon concentration, leading to locally increased mass transport, and, therefore, increased carbon deposition rates.

Other possible reasons for the differences observed in deposits formed by liquid and gaseous precursors include variations in the gas phase or substrate chemistry induced by differences in gas flow and activation mechanisms, which are not investigated in this study.

The objective of this investigation is to determine the effects of mass transport and the presence of oxygen on the diamond CVD system with respect to mass deposition rate, film thickness, and crystal size. Further, attempts are made to isolate the effects of mass transport and the presence of oxygen, to determine the reasons for the differences in growth rate observed in seemingly equivalent diamond CVD systems utilizing liquid and gaseous precursor feedstock.

2. EXPERIMENTAL APPARATUS AND CONDITIONS

Experiments were carried out using a dual-liquid side-injection thermal plasma reactor shown in Fig. 1. The system consists of a DC plasma torch, water-cooled reaction chamber, with ports for two side-injection probes, and a water-cooled substrate holder. The injection probes consist of an inner tube, which carries the precursor, and an outer tube, which carries the atomizing gas. The atomizing gas comes into contact with the precursor only at the tip of the probe. The inner precursor carrying tube and outer atomizing gas tube can also be exchanged to exact control on the average droplet size and atomizing gas velocity. The precursor injection probe is water-cooled, as well, by another set of surrounding tubes. The position of the probe with respect to the substrate can be changed. The torch to substrate distance, however, was kept constant, for all cases, at 25 mm. During deposition the chamber is maintained at 1 atm, with exhaust gases vented from the cooling chamber located below the reaction chamber. The torch is typically run at 300 A and 35 V using a constant current DC power supply, and a torch gas feedrate of 24 and 0.6 slm of Ar and H_2, respectively. Deposition time for all cases was 30 min, which is well above the nucleation time required to form a full diamond film.

Substrates consist of 37.5-mm diameter, 2-mm thick Mo disks, which are bolted unto the copper substrate holder. Silver print is applied to the surfaces between the substrate and copper holder to decrease thermal resistance. Using a set of uniformly spaced thermocouples along the substrate radius, all located 1 mm below the substrate surface, the substrate temperature profile was measured to be $T(r) = 880 - 15.333*r$ °C, where r is the radial distance from the center of the substrate in millimeters. The substrate

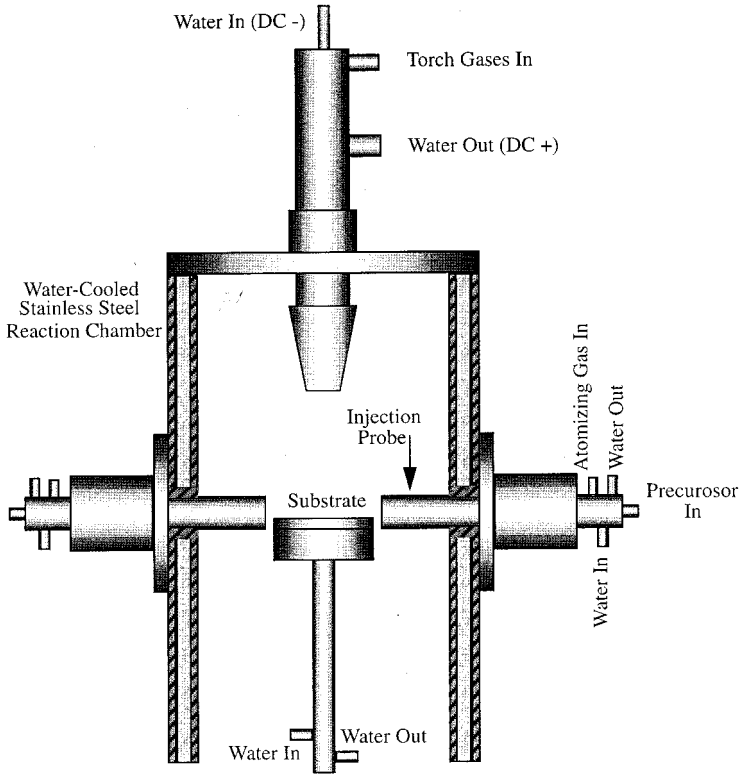

Fig. 1. Dual liquid side-injection thermal plasma reactor.

temperature profile is almost independent of the case conditions tested in this investigation.

In Table I, the system operating conditions for the various cases analyzed in this study are shown. The case names are given in column 1. The precursor and probe gas composition and their respective flowrates are shown in columns 2 and 3, respectively. The carbon to hydrogen and carbon to oxygen mass based ratios are also shown in columns 4 and 5, respectively. These ratios are important in comparing the input rate of carbon compared to the other reactive species in the system. In column 6, the ratio of the Sauters mean diameter (SMD) of the case of interest to the SMD of the A_STAND case is given. The SMD is one of several available measures of average droplet size and merely serves as a guide for relative droplet size comparison. The A_STAND case is used as a comparison of the predicted mean droplet diameter based on the injection probe geometry, against which

Table I. System Operating Conditions

Case	Precursor and probe gas	Flowrate per probe [sccm]	C/H_{mass}	C/O_{mass}	SMD ratio
P_NO	$C_5H_{12} + H_2$	1 + 10,000	0.554	—	13.2
A_O	$C_3H_6O + H_2$	1 + 10,000	0.531	2.250	13.2
M_AR	$CH_4 + H_2 + Ar$	800 + 10,000 + 300	0.371	—	—
CH4	$CH_4 + H_2$	800 + 10,000	0.371	—	—
CH4.II	$CH_4 + H_2$	500 + 10,000	0.243	—	—
A_ARG	$C_3H_6O + H_2 + Ar$	0.8 + 10,000 + 3000	0.393	2.250	0.8
A_STAND	$C_3H_6O + H_2$	0.8 + 10,000	0.393	2.250	1.0

all other probe geometries are compared since it represents the standard liquid case. For cases involving liquid, an increase in the value in column 6 above 1.0 represents an increase in the average droplet size relative to the SMD of the A_STAND case.

The P_NO and A_O cases represent the nonoxygenated and oxygenated liquid cases, respectively. M_AR is the gaseous hydrocarbon case with Ar addition. The CH4 and CH4.II cases are also both gaseous hydrocarbon cases with different methane feedrates. The A_ARG and A_STAND case are comparable oxygenated liquid hydrocarbon precursor cases with and without Ar addition, respectively.

Several diagnostic techniques were used to characterize the thermal plasma system. A laser strobe video system (LSVS) was used to map droplet trajectories in the system. The LSVS consists of a pulsed nitrogen laser (337 nm) which is facing one of the injection probes. A CCD camera outfitted with a monochromatic filter and recording system is used to observe and record droplet trajectories. Finally, deposit surface and cross-section characterization is performed using a JEOL 840II scanning electron microscope (SEM).

3. RESULTS

In order to examine the roles mass transport and the presence of oxygen play in determining growth rates in the liquid and gaseous feedstock cases, a careful examination of deposition results for various operating conditions was undertaken. Operating conditions were chosen to isolate or highlight the effects of either mass transport or the presence of oxygen. Comparisons of the various cases were then performed using the data described below.

Droplet trajectories were mapped using a laser strobe video system for the various liquid precursor cases investigated in this study. Figure 2 shows some characteristic images of droplet trajectories for the liquid precursor

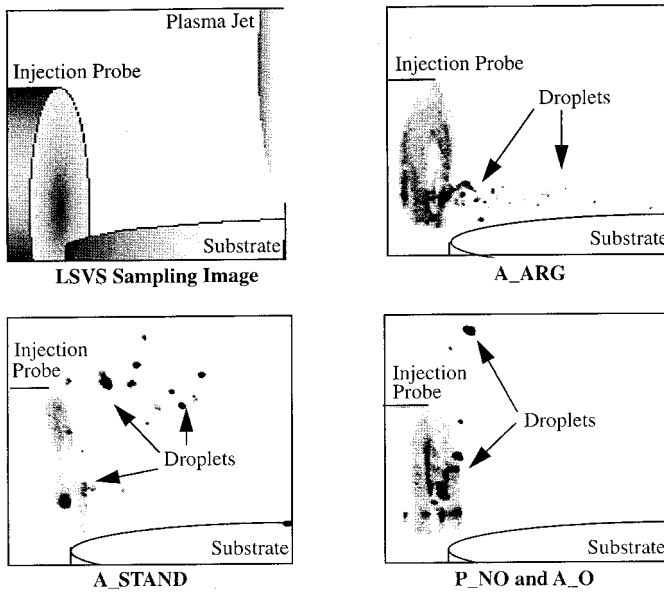

Fig. 2. Laser strobe video system (LSVS) images of droplet trajectories in the liquid feedstock cases. Case label under image relates image to case types in which shown droplet trajectory is applicable.

cases investigated. These images allow a comparison of the droplet trajectories, entrainment point of the liquid into the plasma jet and droplet size distributions for the various liquid feedstock cases analyzed. Samples were also weighed before and after deposition for all cases. Typically, a minimum of three trials were conducted with the same conditions to obtain mass deposition data. Figure 3 shows the average mass deposition rate and standard deviation for the various conditions investigated, ordered for later comparison. SEM was used to obtain surface images of the deposits at various locations, and these images were then used to obtain crystal size data. Figures 4 and 5 show the average crystal size at the substrate center and as a function of radial position for selected samples, respectively. Finally, cross-sectional deposit analysis was undertaken using SEM of the injection plane (IP) and of the plane perpendicular to the injection plane (PIP). The difference in film thickness is more pronounced in the IP than in the PIP, although the shape of the profiles evidence the same trends. Therefore, the former is used for the purposes of comparison. Figures 6 and 7 show the average film thickness as a function of radial position for selected samples.

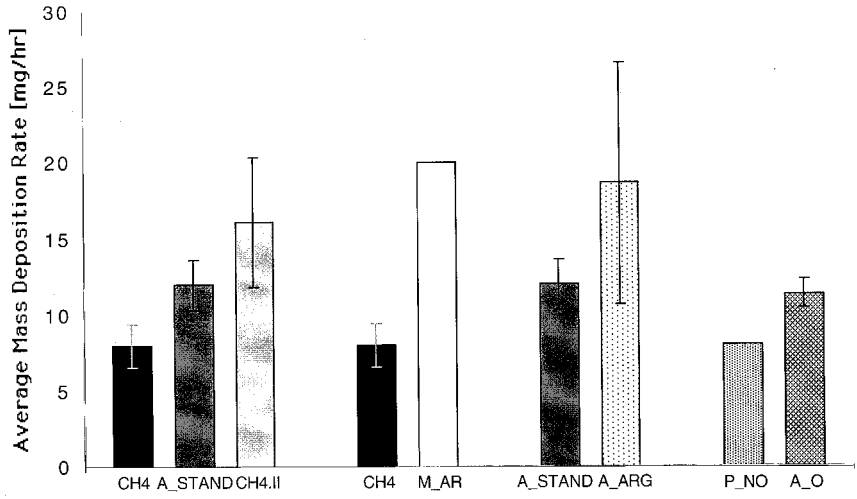

Fig. 3. Average mass deposition rates and standard deviation.

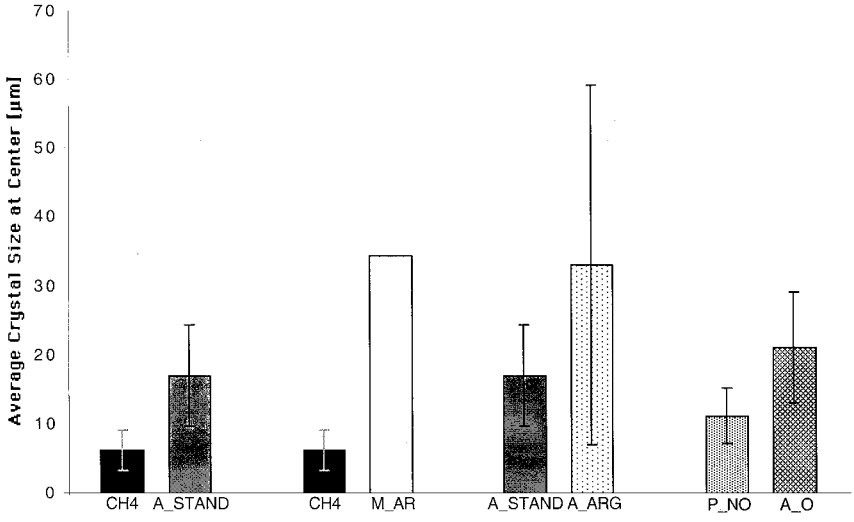

Fig. 4. Average crystal size at substrate center and standard deviation.

4. A COMPARISON OF DROPLET TRAJECTORIES FOR ALL APPLICABLE CASES

The droplet trajectories of the A_STAND case are shown in Fig. 2. Droplets are widely dispersed, centered at an angle of about 45°, with a

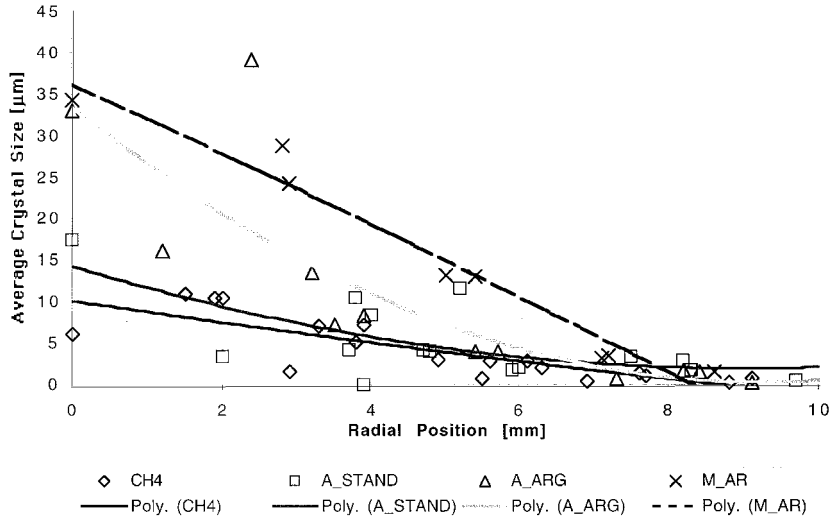

Fig. 5. Average crystal size as a function of radial position in the injection plane for the CH4, A_STAND, A_ARG, and M_AR cases, with polynomial fit.

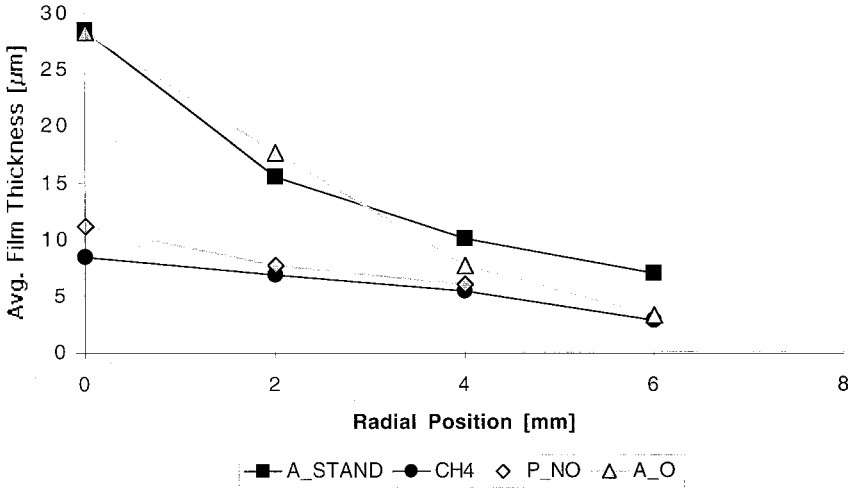

Fig. 6. Average film thickness as a function of radial position for the A_STAND, CH4, P_NO, and A_O cases in the injection plane (IP).

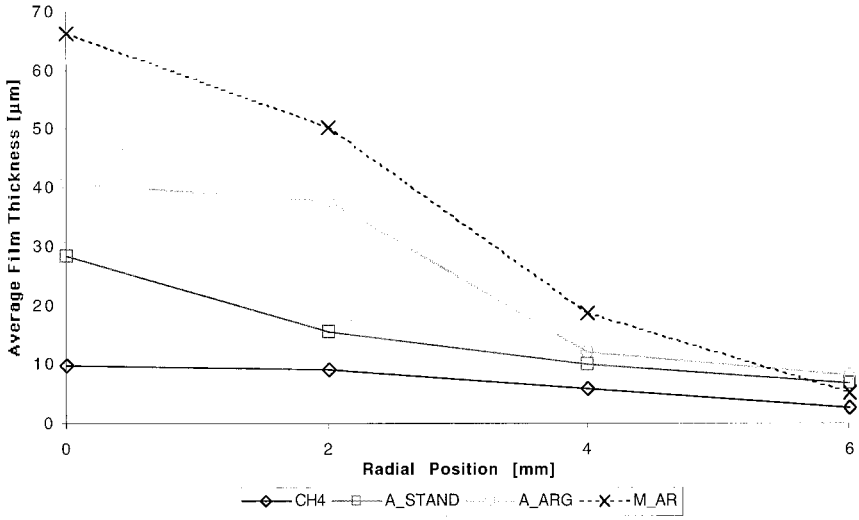

Fig. 7. Average film thickness as a function of radial position in the injection plane for CH4, A_STAND, A_ARG, and M_AR cases.

wide range of droplet sizes. The addition of argon as the atomizing gas to the previous mixture results in much smaller droplets, as can be seen for the A_ARG case. Argon addition provides extra energy for droplet breakup. Further, due to the high momentum of the argon carrier gas, the droplets assume trajectories parallel to the substrate surface. Finally, decreasing the velocity of the atomizing gases, by changing the injection probe geometry, increases the size of the droplets as shown for the P_NO and A_O cases. While it is evident that droplets are larger, the trajectory is also observed to have changed by almost 45° from the A_STAND case. Since the atomizing gas flowrate is lower, the momentum imparted to the droplets in the direction of the plasma jet is reduced as well. Droplets have very little forward momentum and are picked up by the recirculating flow in the reactor. This flow, which starts from the plasma jet, picks up the droplets, and returns them further upstream where they may be entrained in the plasma jet flow.

5. A COMPARISON OF LIQUID AND GASEOUS PRECURSOR USE

A comparison of liquid and gaseous precursor injection diamond CVD has shown that the former results in higher mass deposition rates and larger crystals than the latter. To confirm this observation, deposition using acetone and methane with the same operating conditions and the same carbon feedrate has been undertaken. The CH4 and A_STAND case both have a carbon feedrate of 13×10^{-3} (g-s^{-1}) under the conditions given in Table I.

The mass-based carbon to hydrogen ratio is also similar, 0.371 for the CH4 case and 0.393 for the A_STAND case. This means the amount of carbon and hydrogen available in the system is nearly equivalent for both cases. The molecular composition within which hydrogen and carbon are incorporated is, however, not taken into account. The two primary differences between deposition in these cases, neglecting the aforementioned, is the phase of the liquid as it enters the deposition system, and the presence of oxygen in the liquid case, and the lack thereof in the gaseous case.

A comparison of the average mass deposition rate, shown in Fig. 3, shows that the A_STAND case has an average mass deposition rate significantly higher than that of CH4. A comparison of the average crystal size at the center shows that the A_STAND case has an average crystal size at the center, which is approximately twice as large as that of the CH4 case, as shown in Fig. 4. The film thickness as a function of radial position is shown in Fig. 6 for the injection plane. The film thickness of the CH4 case at the center is approximately one-third the thickness of the A_STAND case at the center. It is also evident from Fig. 6, that the CH4 case films are much more uniform than those of the A_STAND case. Based on this comparison of liquid and gaseous feedstock use, with the same operating conditions and the same carbon feedrate, mass deposition rate, crystal size, and film thickness are all increased in the liquid feedstock case when compared to the gaseous feedstock case.

Several factors in these two systems were not taken into account for the previous comparison. These include the phase of the feedstock as it enters the reaction chamber, the related feeding mechanism, and the oxygen content in acetone. Furthermore, the required activation energy for the two precursors, as well as the reaction pathways, and the concentration of various product species have not been considered. Each of these can play an important part in determining mass deposition rate, film thickness, crystal size, and area of deposit. Exacting control of these parameters is beyond the scope of this study. However another comparison was undertaken to further investigate the differences between deposition with liquid and gaseous precursors.

The A_STAND case was optimized initially for mass deposition rate. However the CH4 case conditions were chosen to allow for a comparison based on the same carbon feedrate and carbon to hydrogen ratio. For a different type of comparison, the methane feedrate was altered to obtain an optimized mass deposition rate for the gaseous precursor case, which would allow for another comparison with the A_STAND case. The CH4.II case, with conditions outlined in Table I, has been found to be the optimal case for mass deposition rate. As can be seen in Fig. 3, the average mass deposition rate for the CH4.II case is much higher than for the CH4 case. The

methane feedrate was 500 sccm for the former, and 800 sccm for the latter, giving C/H_{mass} ratios of 0.243 and 0.371, respectively. These results have been confirmed by a set of five experiments. At first glance, the results seem faulty since a higher carbon feedrate resulting in a smaller mass deposition rate seems contradictory to logic.

A possible explanation for this seemingly faulty observation is based on system optimization related either to the surface or gas phase mechanisms, which enable diamond growth. Graphite deposition may have been enhanced in the CH4 case, and because of high concentrations of atomic hydrogen, higher carbon etching rates may have been realized. Since hydrogen etches graphite at a much higher rate than diamond, particularly at the deposition temperatures in this experiment,[23] an increase in graphite formation may have triggered an increase in the overall carbon etching rate. In addition, since the precursor has been injected directly at the tip of the jet, and much of the energy present there is used to activate the precursor, it is possible that an increase in the methane flowrate may have produced a significant cooling of the jet, thereby effecting lower activation rates for the CH4 case than for the CH4.II case. Finally, gas phase species production may have been altered by the presence of higher methane concentrations, producing less active growth species.

A comparison of the average mass deposition rate of CH4.II and A_STAND cases, shown in Fig. 3, reveals that the average mass deposition rate for the former case is higher than for the latter case. This shows that the carbon feedrate in the reactor system is not necessarily a good indicator of mass deposition rate. The comparison of the CH4.II and A_STAND cases also raises some questions as to the validity of the statement that higher mass deposition rates are possible using liquid rather than gaseous precursors. Other factors, mentioned already, such as the specific processes, which enable activation, the reaction pathways and surface reactions, which differ in these systems, have not been considered in this comparison and may be more important with respect to the mass deposition rate than those factors taken under consideration. Furthermore, while higher mass deposition rates may have been obtained, specification as to the type of deposit, diamond, graphite, or amorphous carbon, has not been addressed. In many potential applications of diamond films, minimizing graphite content is paramount. While previous studies, with similar operating conditions, have confirmed the presence of diamond for these cases,[2] analyses confirming and quantifying graphite presence in the produced deposits using Raman spectroscopy were not undertaken. The claim of having produced diamond films is, therefore, based on previous Raman studies of similar samples and the SEM images, which indicate diamond crystals have been deposited.

The CH4.II case illustrates the effect that making small changes to some parameter in the deposition system can have on the deposit. Furthermore, it illustrates the coupling of effects in the diamond CVD system, which may often produce unexpected results. While investigating the cause of the mass deposition results mentioned above is certain to yield insightful results, the objective of this study remains to determine the effects of mass transport and oxygen presence on the diamond CVD system utilizing liquid and gaseous feedstock. For a comparison of results, operating conditions are being kept equivalent where possible and, for precursor feedrate, equivalent with respect to carbon feedrate. Note that for the cases being compared, the C/H_{mass} ratios are also similar, the objective being to make available in the systems equivalent amounts of carbon and hydrogen. For this reason, further comparisons will be made with respect to the CH4 case, rather than the optimized gaseous precursor (CH4.II) case.

6. MASS TRANSPORT EFFECTS

The effects of increasing mass transport of activated species across the substrate boundary layer are analyzed here. First, a comparison of results when adding Ar as a carrier gas to the gaseous precursor is conducted. The M_AR and CH4 cases are representative for comparison. Adding 3 slm of Ar to the typical 800 sccm of methane is believed to increase precursor feeding to the primary activation region of the system, namely, the tip of the thermal plasma jet. This statement is supported both by a model of the CVD system, described elsewhere,[18–20] as well as by the difference Ar addition makes in the droplet trajectories, shown in Fig. 2. Higher feeding rates of precursor to the activation region is believed to result in higher activation rates, assuming sufficient energy is available. With higher activation rates, mass transport of the active species across the substrate diffusion boundary layer is enhanced, resulting in higher growth rates.

A comparison of the M_AR and CH4 cases reveals that the average mass deposition rate in the former case is nearly three times that of the latter case, as shown in Fig. 3. Further, we see in Fig. 5 the average crystal size as a function of radial position. The decrease in crystal size is much faster for the M_AR case than for the CH4 case with radial position. This indicates a more uniform surface in the CH4 case. From Fig. 4, it is evident that the average crystal size at the center for the M_AR case is about six times that of the latter case. Finally, a comparison of film thickness as a function of radial position in the injection plane, shown in Fig. 7, reveals that the film thickness at the center of the M_AR case is about two times the thickness at the center compared to the CH4 case. We also see that for the CH4 case, no film was found in the cross-sectional SEM past 4 mm, while diamond film is still evident for the M_AR case up to 6 mm.

Next, a comparison of results is conducted when adding Ar as a carrier gas to the liquid precursor. The A_STAND and A_ARG case are representative of liquid injection without Ar addition and liquid injection with Ar addition, respectively. Operating conditions are equivalent in both cases, save the addition of 3 slm of Ar in each probe in the A_ARG case. The effect that this addition has on droplet trajectories can be seen in Fig. 2. The flow in the A_ARG case is parallel to the substrate, counter to the direction of plasma gas flow over the substrate. The droplets are also much smaller and much higher in number. In the A_STAND case, we see that droplets are dispersed over a large solid angle centered at approximately 45° upward of the substrate. Therefore, precursor entrainment in the A_STAND case, as well as activation, are most likely lower than in the A_ARG case.

As is shown in Fig. 3, the average mass deposition rate for the A_STAND case is lower than for the A_ARG case. A comparison of average crystal size as a function of radial location, shown in Fig. 5, reveals that the average crystal size for the A_STAND case is significantly lower than for the A_ARG case. Furthermore, the average crystal size for the A_ARG case drops off much faster than that of the A_STAND case with distance from the center of the substrate. This is believed to be related to the active species distribution over the substrate area in each respective case. Although the initial drop-off in crystal size for the A_ARG case is large in the 2–6 mm range of the substrate radial position, small crystals are still evident out to nearly 10 mm. A comparison of the average film thickness as a function of radial position, shown in Fig. 7, shows results similar to the average crystal size. The film thickness A_ARG case is larger at the center when compared to the A_STAND case, then drops off rapidly between 2–6 mm in the radial direction. Both the film thickness and average crystal size as a function of radial position data, shows that the A_STAND film is more uniform over the substrate area than the A_ARG case.

Although the data above does not conclusively show that the addition of Ar increases mass transport of active growth species across the substrate diffusion boundary layer, the data can be interpreted to support this hypothesis. The only difference when comparing the A_ARG to the A_STAND case and the M_AR to the CH4 case is the addition of Ar. None of the other factors which have affected comparisons between deposits produced with different precursors, apply in this case. With the addition of Ar, we observe thicker films at the center of the substrate, larger average crystal size, and a higher mass deposition rate, regardless of the use of a liquid or gas phase precursor.

Modeling efforts of this reactor and the laser strobe video images captured of droplet trajectories in the A_STAND and A_ARG cases, support

the hypothesis that larger amounts of precursor feedstock reach the boundary layer when adding Ar, than when Ar is not added. Provided that the precursor is entrained in the thermal plasma jet close to the substrate and is activated there, at a higher rate in the cases with Ar addition, would translate into higher local mass transport rates for those species produced in the activation process. Since these precursor species would most likely consist of hydrocarbons along with atomic hydrogen and, in the acetone cases OH and O radicals, growth rates at the surface would increase assuming sufficient other species for surface activation, namely atomic hydrogen, is present. Modeling of the dual-side injection system has shown that the growth process is limited by mass transport of carbonaceous species and that sufficient atomic hydrogen is present. Therefore, an increase in those species translates into a local increase in growth rate.

7. THE EFFECT OF OXYGEN ON THE DIAMOND CVD SYSTEM

To determine the effect of oxygen on the liquid diamond CVD system, the use of pentane (C_5H_{12}), case P_NO, and acetone (C_3H_6O), case A_O, were compared with all the same operating conditions. Comparisons are again based on systems with equivalent carbon feedrates. Pentane was chosen, because the C/H_{mass} of both acetone and pentane for equivalent flow rates were similar, 0.531 and 0.554, respectively. Again, consideration of the activation mechanism and the activation energy required has been neglected in this comparison.

As can be seen in Fig. 6, the average film thickness in the injection plane of the cases with oxyen is larger than for those without oxygen. In Fig. 3, we see the average mass deposition rate for the P_NO case is significantly lower than in the A_O case. While the A_STAND case has a larger mass deposition rate than the CH4 case, the CH4.II case has the highest rate of the three. This would indicate that the presence of oxygen in acetone is not necessarily responsible for the higher mass deposition rate observed in oxygenated liquid precursors when compared to nonoxygenated gaseous precursors. Without further investigations, to determine gas phase species concentrations and reactions, certainty as to the effect of oxygen presence in this system can not be given. Overall, a comparison of cases with and without oxygen, with all controlled operating conditions the same, and based on equivalent carbon feedrates and hydrogen, indicate that the growth rates in the former case are higher than in the latter. However the activation energies and reaction pathways have not been taken into account in this comparison, so the results may be apparitions of these factors. Further details of this part of the study can be found elsewhere.[24]

8. CONCLUSIONS

The objective of this study has been to evaluate two of the possible effects believed responsible for increased growth rate in the liquid precursor case, namely, mass transport and the presence of oxygen. This study shows that by optimizing the deposition conditions with respect to the precursor of interest, similar mass deposition rates can be obtained using a gaseous precursor, as are obtained with liquid precursors. Laser strobe video images show that droplets injected from the precursor probes do reach the plasma jet, producing regions of highly concentrated activated species when entrained in the plasma jet. The addition of Ar as an atomizing gas is also shown to increase precursor entrainment by direct injection into the thermal plasma jet tip.

Mass transport rates of active growth species are believed to be enhanced with the addition of Ar as an atomizing gas. Both for the gaseous and liquid precursor cases. Ar addition results in higher mass deposition rates, larger crystal size, and thicker films. Supported by laser strobe video images and a process model described elsewhere,[18–20] the hypothesis is put forth that the enhancements observed in the system with Ar carrier gas addition is due to an increase in the mass transport of active growth species across the substrate diffusion boundary layer. The Ar gas allows for higher activation rates as more of the precursor is brought into contact with those areas of the jet which enable activation.

The effect of oxygen on the diamond CVD system is difficult to evaluate because the required activation energy and product species depend on the type and molecular structure of the precursor chosen. Furthermore, the results obtained when comparing cases with equivalent carbon feedrate do not hold when comparing cases optimized for mass deposition rate. The use of acetone was considered as the oxygenated liquid feedstock and, compared to the use of methane, a gaseous hydrocarbon, and pentane, a liquid hydrocarbon. Results show that the mass deposition rate, film thickness, and crystal size are all enhanced for the oxygenated liquid feedstock case when comparison is based on equivalent carbon feedrates. Comparison of the nonoxygenated liquid case with the nonoxygenated gaseous case indicates little difference in growth rates, which supports the statement that precursor phase is not a significant factor in determining growth rates for the thermal plasma diamond CVD system. These results, however, are only applicable to the specific precursors used and do not necessarily represent the effects in all comparisons of oxygenated liquid precursors versus hydrocarbon liquid and gaseous precursors. For a more complete analysis, the individual reaction pathways, the resulting species concentrations, and the available energy in the individual system would need to be modeled.

ACKNOWLEDGMENTS

This research was supported by the Engineering Research Program of the Office of Basic Energy Sciences at the U.S. Department of Energy under grant No. FG02-85ER-13433.

REFERENCES

1. Q. Zhuang, P. Schwendinger, C. Hammerstrand, J. Heberlein, E. Pfender, and R. Young, *Proc. Intern. Symp. Plasma Chem.* **12**, 2303–2308 (1995).
2. M. Asmann, C. F. M. Borges, J. Heberlein, and E. Pfender, *Proc. Intern. Symp. Plasma Chem.* **13**, 1206–1211 (1997).
3. C. George, C. Hammerstrand, D. Kolman, P. Schwendinger, D. Zhuang, J. Heberlein, and E. Pfender, *Plasma Technology for Low-Cost Diamond Deposition*, final report submitted to Westinghouse Science and Tecnology Center, University of Minnesota—High Temperature Laboratory (1994).
4. Q. Y. Han, T. Or, Z. Lu, J. Heberlein, and E. Pfender, *Proc. 2nd Intern. Symp. Diamond Materials* **91-8**, 115–122 (1991).
5. T. Or, Q. Y. Han, Z. Lu, J. Heberlein, and E. Pfender, *Proc. Intern. Symp. Plasma Chem.* **10**, 3.1–15 (1–6) (1991).
6. E. Pfender, Q. Y. Han, T. Or, Z. Lu, and J. Heberlein, *Diamond Related Mater.* **1**, 127–133 (1992).
7. J. Heberlein and E. Pfender, *Mater. Sci. Forum* **140–142**, 477–496 (1993).
8. S. Paik, X. Chen, P. Kong, and E. Pfender, *Plasma Chem. Plasma Process.* **11**, 229–249 (1991).
9. Y. Liou, A. Inspektor, R. Weimer, D. Knight, and R. Messier, *J. Mater. Res.* **5**, 2305–2312 (1990).
10. S. Kapoor, M. Kelly, and S. Hagstroem, *J. Appl. Phys.* **77**, 6267–6272 (1995).
11. T.-H. Kim and T. Kobayashi, *Jpn. J. Appl. Phys.* **33**, L459–L462 (1994).
12. L. Schaefer and C. Klages, *Surface Coat. Technol.* **47**, 13–21 (1991).
13. J. Mucha, D. Flamm, and D. Ibbotson, *J. Appl. Phys.* **65**, 3448–3452 (1989).
14. Y. Muranaka, H. Yamashita, and H. Miyadera. *Surf. Coat. Technol.* **47** (1991).
15. S. Jin, R. Molnar, D. Jong, and T. Moustakas, *Diamond Optics V*, **1759**, 41–49 (1992).
16. S. Jin and T. Moustakas, *Diamond Related Mater.* **2**, 1355–1359 (1993).
17. U. Meier and L. Hunziker, *Proc. Intern. Symp. Diamond Mater.* **10**, 203–208 (1991).
18. D. Kolman, J. Heberlein and E. Pfender, *Proc. Intern. Symp. Plasma Chem.* **13**, 320–325 (1997).
19. D. Kolman, J. Heberlein and E. Pfender, *Plasma Chem. Plasma Process.* **18**, 73–89 (1998).
20. D. Kolman, J. Heberlein and E. Pfender, *Diamond Related Mater.* **7**, 794–801 (1998).
21. J. Rankin, R. E. Boekenhauer, R. Csencsits, Y. Shigesato, M. W. Jacobson, and B. W. Sheldon, *J. Mater. Res.* **9**, 2164–2173 (1994).
22. J. Rankin, Y. Shigesato, R. E. Boekenhauer, R. Csencsits, D. C. Paine, and B. W. Sheldon, *Mater. Res. Soc. Symp. Proc.* **270**, 317–322 (1992).
23. W. Hsu, D. M. Tung, E. A. Fuchs, and K. F. McCarty, *Appl. Phys. Lett.* **55**, 2739–2741 (1989).
24. M. Asmann, K. Nelson, J. Heberlein, and E. Pfender, *Proc. Intern. Symp. Plasma Chem.* **14**, August, 1999, to be published.